DTU Library

Two-dimensional elliptically shaped electromagnetic vibration energy harvester

Imbaquingo, Carlos; Bahl, Christian; Insinga, Andrea R.; Bjørk, Rasmus

Link back to DTU Orbit

Citation (APA):
Imbaquingo, C., Bahl, C., Insinga, A. R., & Bjørk, R. (2023). Two-dimensional elliptically shaped electromagnetic vibration energy harvester. *Sensors and Actuators A: Physical*, *350*, Article 114091. https://doi.org/10.1016/j.sna.2022.114091

Two-dimensional elliptically shaped electromagnetic vibration energy harvester

Carlos Imbaquingo *, Christian Bahl, Andrea R. Insinga, Rasmus Bjørk

Department of Energy Conversion and Storage, DTU Energy, Kongens Lyngby, 2800, Denmark

ARTICLE INFO

ABSTRACT

An elliptically shaped electromagnetic vibration energy harvester is presented for two- and one-dimensional motions with the easy tuning of the resonance frequency. The harvester consists of a free-to-move ring-shaped permanent magnet with radial magnetization, a set of cube magnets distributed elliptically in a fixed holder, and two coil windings located above and below the harvester. When the device is exposed to vibrations, the free-to-move ring magnet moves until the magnetic restoring force from the fixed cube magnets pushes it back while inducing an electromagnetic force on the fixed coils. The performance of the device is characterized using an XY-shaker, whose frequency is swept from 1 Hz to 10 Hz with motion amplitudes of 2 mm and 4 mm on both axes simultaneously. Unlike 1-D harvesters, the resulting output power shows two resonant frequencies at 4.5 Hz and 7 Hz, at which the harvester can generate around 1.5 mW. The device also displays a nonlinear hardening resonator behaviour. Finally, 1D vibration experimental results show that the output power of the prototype depends on its angular position with respect to the motion direction of the vibration source, reaching a maximum at an angular position of 45°.

1. Introduction

Interest in energy harvesting for low power and Internet-of-Things (IoT) devices has increased substantially to save on battery replacement and also reduce the use of non-regulated contaminants in currently-used batteries as some of these can be environmentally problematic [1]. Fortunately, due to advances in electronic technologies, the power requirement of IoT devices has been reduced to a point where extracting energy from the surroundings could supply enough power for such units [2]. Energy can be harvested from several different environmental sources [3], but one all-around source is vibrational energy. Piezoelectric, electrostatic or electromagnetic energy harvesters are transducer mechanisms that use this energy source. For electromagnetic vibration energy harvesters (EMVEH), different approaches and topologies have been studied, with an overview of devices presented in Ref. [4], with prototypes classified in terms of boundary conditions, magnetic and mechanical design, manufacturing aspects, excitation type and direction of excitation.

The problem with existing EMVEHs is that the harvested power is limited to a relatively narrow bandwidth around their resonant frequency [5]. Thus such devices need to be designed precisely to match the vibration frequency of the structure to which they will be attached. This limitation of bandwidth is a consequence of the overall design of EMVEHS, namely their limitation by Earnshaw's theorem,

which requires that one or two direction(s) of motion have to be restricted. As a result, almost all EMVEHs harvest energy from one-dimensional motion [6] with the inherent limitations of device design and functionality that this results in [7].

A typical one-dimensional EMVEH is designed with three co-axial magnets with opposite polarities, such that the middle magnet is floating and free to move relative to a set of coils [8–14]. The magnet force in this configuration is a spring-like restoring force on the middle magnet [11]. This is superior to mechanical springs etc., which can wear out with extended use. Current devices are in the centimetre range and produce a voltage in the mV-V range and power in the μW-mW range [6], although this depends on the exact way that the device is operated as EMVEH devices can have a quite complex phase space [15,16]. It should also be mentioned that less conventional designs exists, such as magnet-on-a-spring [17], rolling magnets [18,19], soft magnetic composites [20], roly-poly-like devices [21], magnetic pendulums [22,23] and Halbach devices [24].

This work hypothesizes that a broader and more easily tuneable bandwidth can be realized by allowing an EMVEH to vibrate in more than one direction. Such an EMVEH could harvest both vibrations from true two-dimensional vibrations or be designed such that even one-dimensional vibrations can result in internal two-dimensional motion of the EMVEH, with a potentially broad frequency range as a result.

At present only a few EMVEH designs have considered two-dimensional motion, here called 2D-EMVEHs. In the 2D-EMVEH the movement of the free magnet will not be along a line, as for traditional 1D-EMVEHs, but rather on a plane. However, the free magnet will still have to be confined by surfaces above and below the place of movement to prevent the free magnet from flipping over. A number of devices that have 2D movement of the free-to-move magnet but where the device was only tested with one-dimensional vibrations exists. One is the device presented in Ref. [25] which considers two-dimensional movement, however with the sole purpose of mitigating the known friction issues in EMVEHs, but not to harvest energy from actual two-dimensional motion and the device is only tested for one-dimensional vibrations. Likewise, Ref. [26] presents a design where a floating magnet can move in two dimensions, but the device was only tested with one-dimensional vibrations. Another harvesting system that can have internal rotary 2D motion is presented in Ref. [27] that demonstrates a spherical magnet system with said magnet inside a capsule wound with two coils. However, as there is no repulsive force in the capsule, this harvester needs stoppers on its inner walls to prevent the spherical magnet from breaking. Another 2D harvesting system is the design presented in Ref. [28], where a eccentric mass in oscillatory motion can under certain conditions be made to rotate in a 2D pattern. Finally, in a recent publication, the authors of this work presented a two-dimensional electromagnetic vibration harvester with variable magnetic stiffness and electromagnetic damping [29]. This device has a free-to-move cylindrical magnetic structure with a set of bearings located on top and bottom, a couple of coils located on top and bottom of the device and finally a fixed system of disc-shaped magnets placed inside a ring holder. However, contrary to the device presented in this work, the harvester in Ref. [29] is round and does not have any shape asymmetries that results in different internal resonance frequencies.

The two-dimensional electromagnetic harvesters discussed above are first-generation devices and there are many points unexplored in these devices. Primary of these is whether two-dimensional harvester can potentially offer a broader frequency range that can be harvested, by changing and tuning their internal shape to allow for multiple resonance frequencies. This has not been explored previously in the any of the references mentioned above. In the harvester proposed in this work, we change the shape of the two-dimensional harvester to have two different resonant frequencies, to realize a potentially broadband harvester. We quantify the behaviour of such a harvester for a range of frequencies and motion amplitudes for both one- and two-dimensional movements to understand the frequency harvesting bandwidth of such asymmetric two-dimensional harvesters.

2. Design of the 2D-EMVEH

As stated above, we in this work consider a geometrically asymmetric two-dimensional harvester. A schematic and a picture of the prototype investigated in this work are depicted in Figs. 1 and 2, respectively. The device consists of three main parts. The first part is a free-to-move ring-shaped permanent magnet with radial magnetization and with bearings placed on the top and bottom. These bearing are made of a non-magnetic material, here plastic. The second part encapsulates the moving magnet and consists of a set of cube magnets distributed elliptically in a fixed structure. As a permanent magnet in an elliptical shape is not available commercially, an elliptically-shaped holder was 3D-printed, into which cube magnets were inserted and distributed at equal angles. Their north poles face the inner side, creating an elliptically-shaped magnetic structure. The third part is a pair of coils placed above and below the harvester. The dimensions and component specifications of the harvester are listed in Table 1. The specific dimensions are chosen based on available dimensions of the ring magnet, which is radially magnetized, but also based on a principle to show a working device. Thus the design parameters for the system could undoubtedly be optimized, i.e. we stress that the
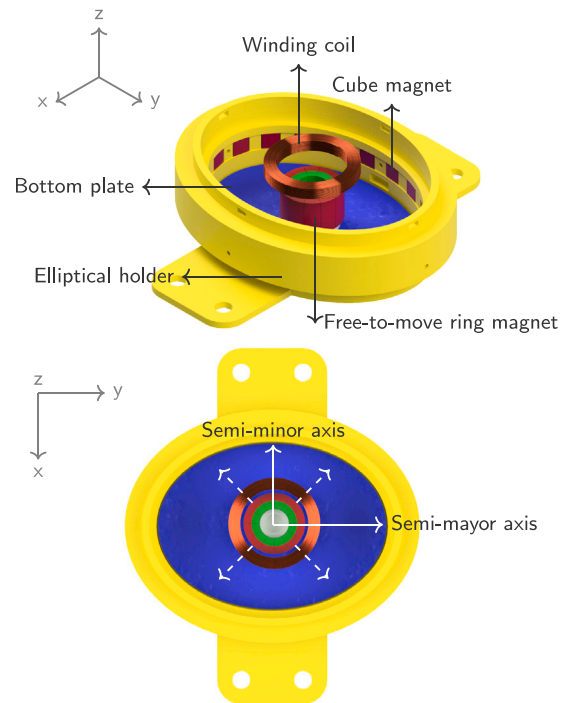

Fig. 1. Schematic of the two-dimensional electromagnetic energy harvester in both isometric and top view. A 280-turn coil is shown on top and a similar coil is located below the plane of movement. The lengths of the semi major and minor axis of the harvester are 119 mm and 95 mm respectively (the blue area). The direction of magnetization is indicated by colour, with red corresponding to north and green to south. The north on the outside of the free-to-move ring magnet thus faces the north of the cube magnets in the elliptical holder, creating magnetic repulsion. (For interpretation of the references to colour in this figure legend, the reader is referred to the web version of this article.)
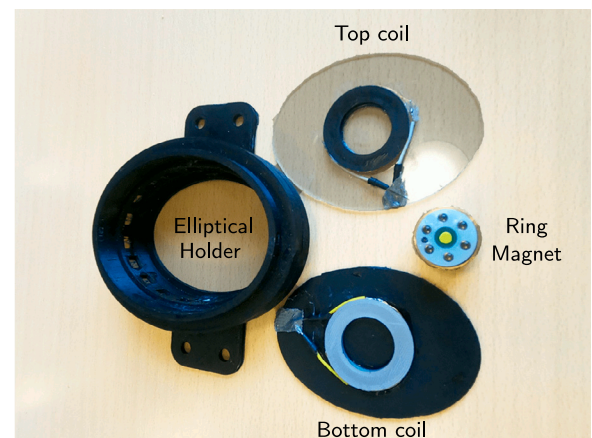

Fig. 2. The actual 2D-EMVEH prototype. The ring magnet has the bearing BB-626TW-B180-GL fixed on top of it.

prototype demonstrated here is to explore the working principle of a 2D harvester, not to produce an optimal device.

The design was built around a commercially available radial-flux ring magnet, here with a radius of 25 mm. Following this, the magnetic force between this magnet and the set of cube magnets was modelled using a finite element framework to select appropriate dimensions of the ellipse, i.e. to ensure that the intensity of the restoring force is sufficient for the interaction between the ring and cube magnets to cause the system to behave as a hard spring resonator. A previous design suggests a restoring force of around 10 N is appropriate for

Table 1
Dimensions and component specifications.

Component	Parameter	Quantity
Ring magnet	Inner radius	12 mm
	Outer radius	25 mm
	Height	14 mm
	Grade	NdFeB, N50
Cube magnets	Amount	20
	Length	7 mm
	Grade	NdFeB, N42
Coil windings	Amount	2
	Inner radius	27 mm
	Outer radius	40 mm
	Height	2.5 mm
	Number of turns	280
	Wire gauge	0.202 mm
	Resistance	16.5 Ω
	Inductance	3.35 mH
Elliptical holder	Semi minor axis	95 mm
	Semi major axis	119 mm
	Height	32.75 mm

Fig. 3. Schematic cross-section of the 2D-EMVEH and magnetic flux lines between the cube magnets in the elliptical holder (left and right) and the radial-flux ring magnet (centre). The winding coils located above and below the plane of movement of the ring magnet are also shown.

a ring magnet of the given size [12]. A stronger force would lead to an excessively rigid system and a weaker force to an excessively loose one, with both cases resulting in low or no power being generated. The lengths of the semi-major and semi-minor axes, detailed in Table 1, give a suitable restoring force of 9 N and 8.1 N, respectively, when the ring magnet is at the proximity of the axes edges, as will be discussed in further detail in the results section.

Likewise, the coil size depends on the dimensions of the ring magnet. According to Ref. [6], the inner diameter of the coil has to be a bit larger than the outer diameter of the ring magnet. Furthermore, the outer diameter and thickness of the coil winding are small enough so that every turn contributes to inducing a voltage. Otherwise, the outer and top turns would not see the rate of change of the flux, so no induced voltage is generated, resulting in a higher coil winding internal resistance.

According to Earnshaw's theorem, there is no free-space point of stable equilibrium for a paramagnet or ferromagnet in a magnetic field [30]. Still, stability can be attained if the magnet is constrained to move in one or two dimensions. Here, in order to allow movement in two dimensions, the ring magnet is confined by a top and bottom plate, which thus prevents tilting of the ring magnet. To allow for easy movement, i.e. decrease the friction of the ring magnet on the plates, the ends of the ring magnet are fitted with non-magnetic ball-bearings (Thrust washers, BB-626TW-B180-GL from IGUS). In general, the lower the friction of the ring magnet, the less power is dissipated as heat in the device.

When the harvester is exposed to a vibrating ambient source, the relative position of the ring magnet changes until the magnetic restoring force from the magnetic interaction between the ring and cube magnets in the elliptical holder pushes it back. This is illustrated in the cross-section area of the system shown in Fig. 3, where the flux lines can also be seen inducing an EMF in the coil windings.

2.1. Physics of the 2D-EMVEH

Overall the physics of the 2D-EMVEH is similar to that of 1D-EMVEHs devices, and the same equation of motion applies, except that the motion now occurs in two dimensions and the magnetic force depends on the (x, y)-position of the free-to-move magnet. Likewise, the electromagnetic damping from the coil windings is also similar to 1D-EMVEH models [12,31], which depends on the relative position of the free-to-move magnet with respect to the coil winding. Thus, the 2D-EMVEH is like the 1D-EMVEH, a magnetic spring-like system with a damping force from the coil windings.
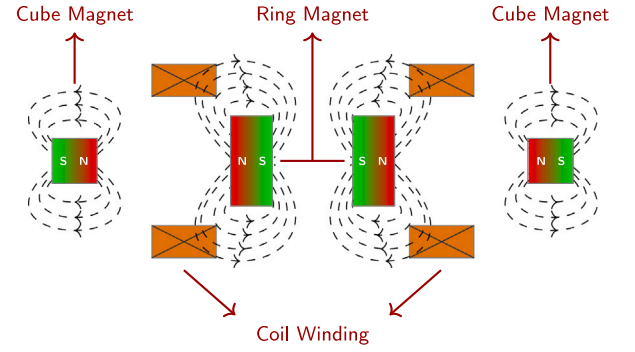
In 1D an EMVEH harvester is governed by the following sets of equations [16]:

$$m_{free}\ddot{z} = F_{coil}(z, \dots, I_n, \dots)$$
$$+ F_{mag}(z) + F_{g,z} + F_{frict}(\dot{z}) \tag{1}$$

$$L_n \dot{I}_n + \sum_{n'} L_{n,n'} \dot{I}_{n'} + R_n I_n + \dot{z}\frac{d\phi_n}{dz_n} = 0, \tag{2}$$

where z is the position variable, m_{free} is the mass of the free-to-move magnet, F_{coil} is the force due to the interaction of the free-to-move magnet with the coils, F_{mag} is the force due to the interaction of the free-to-move magnet with the fixed magnets, $F_{g,z}$ is the gravitational force in the direction that the harvester is positioned and $F_{frict} = -c\dot{z}$ is a friction force. The second equation, which determines the electrical condition of a coil winding, is stated for the n_{th} coil winding, but an equation exists for every independent coil winding. For the n_{th} coil winding, a current I_n is running, and where L_n is the self-inductance of each coil, $L_{n,n'}$ is the mutual inductance between the n_{th} and n'_{th} coils, R_n is the resistance connected to each coil winding, and ϕ_n is the magnetic flux density through the coil. This is the most general form of the governing equation for a 1D-EMVEH. If the coil windings are connected in series, the system of equations reduces as only one current and one resistance is present.

In 2D, the harvester will be able to move in both the x and y directions. This means that the magnetic force will depend on both the x and y coordinates, and the coil force will depend on the x and y coordinates as well as the velocities in the two directions, i.e. v_x and v_y. Regarding the changing flux through a coil in the 2D-EMVEH, as the free-to-move magnet will now no longer pass through a coil winding, but instead above or below it, the position variable is changed to the distance between the free-to-move magnet and the coil winding. Calling this distance r, the equations of motion for the 2D-EMVEH is:

$$m_{free}\ddot{x} = F_{coil,x}(x, y, \dots, I_n, \dots)$$
$$+ F_{mag,x}(x, y) + F_{g,x} + F_{frict,x}(\dot{x}) \tag{3}$$

$$m_{free}\ddot{y} = F_{coil,y}(x, y, \dots, I_n, \dots)$$
$$+ F_{mag,y}(x, y) + F_{g,y} + F_{frict,y}(\dot{y}) \tag{4}$$

$$L_n \dot{I}_n + \sum_{n'} L_{n,n'} \dot{I}_{n'} + R_n I_n + v_{dir}\|v_\|\|\frac{d\phi_n}{dr_n} = 0 \tag{5}$$

Again there is a differential equation for each independent coil winding, but only the n_{th} equation is given. We in this work operate the harvester horizontally, so $F_{g,x} = F_{g,y} = 0$. The velocity $v_\|$ is the
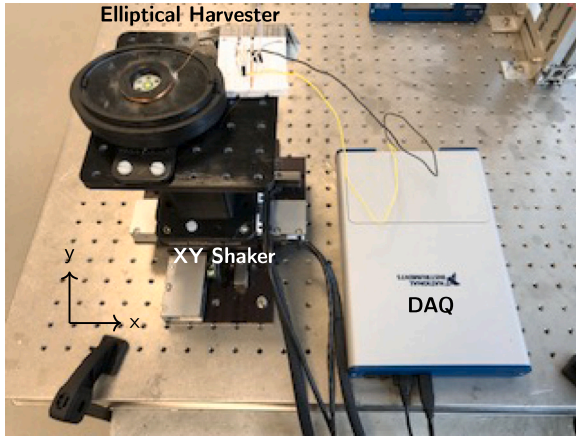
Fig. 4. Experimental setup showing the XY-shaker, with the energy harvester on top and the data acquisition card aside.

velocity parallel to the position vector r connecting the free-to-move magnet and the coil winding, i.e. the line between the free-to-move magnet and the coil winding. The direction v_{dir} indicates if the free-to-move magnet is moving towards or away from the coil winding. The parallel component of the velocity ensures that a permanent magnet moving in a circle around a coil winding will not induce a current on it, as the instantaneous velocity will, in this case, always be parallel to the r-vector.

The vector between the free-to-move magnet and the coil winding is the relative distance, which is thus given by $x_{rel} = (x_c - x_f)$ and $y_{rel} = (y_c - y_f)$, where the free-to-move magnet has coordinates (x_f, y_f) and is moving with a velocity (v_x, v_y) relative to the coil winding, and the coil winding has coordinates (x_c, y_c). The distance r is thus $r = \sqrt{x_{rel}^2 + y_{rel}^2}$

The parallel component of the velocity in the $x-$ and $y-$directions are thus

$$\begin{bmatrix} v_{\parallel,x} \\ v_{\parallel,y} \end{bmatrix} = \frac{v_x x_{rel} + v_y y_{rel}}{x_{rel}^2 + y_{rel}^2} \begin{bmatrix} x_{rel} \\ y_{rel} \end{bmatrix} \quad (6)$$

And the direction of the velocity of the free-to-move magnet towards or away from the coil winding as given by v_{dir} is

$$v_{dir} = \frac{v_{\parallel,x} x_{rel} + v_{\parallel,y} y_{rel}}{|v_{\parallel,x} x_{rel} + v_{\parallel,y} y_{rel}|}$$

$$v_{dir} = \text{sign}\left(v_{\parallel,x} x_{rel} + v_{\parallel,y} y_{rel}\right) \quad (7)$$

This will be equal to $+1$ when the magnet moves towards the coil winding and -1 when it moves away from the coil winding.

While the magnetic force can be found using a finite element framework for a specific device geometry, the coil winding force must consider the relative distance mentioned above, i,e. the coil winding force on the free-to-move magnet from the n_{th} coil winding is given by

$$F_{coil,x,n}(\dot{x}, x, \dot{y}, y, I_n) = I_n \frac{d\phi_n}{dr_n} \frac{x_{rel,n}}{\sqrt{x_{rel,n}^2 + y_{rel,n}^2}} \quad (8)$$

$$F_{coil,y,n}(\dot{x}, x, \dot{y}, y, I_n) = I_n \frac{d\phi_n}{dr_n} \frac{y_{rel,n}}{\sqrt{x_{rel,n}^2 + y_{rel,n}^2}} \quad (9)$$

and the total force is just the sum from all coil windings.

The derived mathematical model will be subsequently compared with experimental results. In future works, such a validated model could also be used to design an optimal harvester. However, as stressed previously, that is not the goal of this work.

3. Results

In the following, the movement and induced power of the 2D-EMVEH prototype are investigated when this is subjected to vibrations in both one and two dimensions.

The experimental setup used for vibrational testing of the 2D-EMVEH is illustrated in Fig. 4. A two-dimensional shaker was employed to generate the vibration source. The shaker is a SRS-004-006–004-003-01-XY from H2 W Technologies, which has two platforms that move independently, perpendicular to each other, resulting in a two-dimensional motion that follows Lissajous patterns, i.e. where the movements in the two directions are independently given by sinusoidal curves that may have different frequencies. A custom LabVIEW interface controls the shaker. The output voltages of the coil windings were measured and saved at a sampling frequency of 1 kHz by a data acquisition card (USB-6351 from National Instruments). The coil windings were connected in series to attain a larger output voltage, and a load that matches their combined internal resistance was employed to ensure that the maximum power transfer is obtained [32].

3.1. 2D vibrations

An experiment was performed where the 2D-EMVEH was placed such that the semi-major axis of the elliptical holder is aligned to one of the motion directions of the shaker platform as shown in Fig. 4. Always starting from rest, the harvester was then subjected to a sinusoidal vibration in the $x-$ and $y-$directions with a frequency between 1 and 10 Hz on the $x-$direction (semi-major axis) in steps of 0.25 Hz and a frequency between 1 and 10 Hz on the $y-$direction (semi-minor axis) in steps of 1 Hz with an amplitude motion of 2 mm on each platform. Additionally, a similar experiment was performed with an amplitude motion of 4 mm on each platform and a maximum frequency of 8 Hz due to the mechanical limitations of the XY shaker. It is stressed that the system started from rest for each frequency tested. The reason for this is that EMVEH harvesters are known to display hysteric behaviour if subjected to a changing frequency, i.e. the state in terms of power production and movement that the system ends up in depends on the history of frequencies that the harvester has been exposed to [8,16,31,33]. To avoid this dependency here, each experiment at a given frequency is started from rest.

Note that, in this work, it was explicitly decided on a full laboratory test of the vibrational harvester, instead of testing this in various applications. While the harvester would be suited for vibrations sources such as bicycle riding, human motion, and car riding [34], mounting the harvester on these applications makes the measurements essentially unreproducible. However, using a standard XY shaker in a laboratory setup to test the harvester, the experiments can readily be reproduced and used as a comparison by other researchers. Also note that the harvester is tested in a horizontal configuration, to ensure that the device is symmetric in the two shaking directions. While most harvesters are employed vertically, and this harvester could easily also be so, the additional asymmetry introduced by the gravitational field is not desired in the experiments done here. However this will not have a large impact on the device, as the free-to-move ring magnet only has a mass of 38 g, and it thus only experiences a gravitational force of 0.37 N, which is small compared to the magnetic force calculated previously.

For each experiment the voltage was recorded for a period of 3 s after the system reached a steady state. Fig. 5 shows the output voltage as a function of time for the top and bottom coil windings, connected in series, for an experiment with frequencies of 3.5 Hz and 6 Hz for the semi-minor and semi-major axes, respectively, and an amplitude of 4 mm on both axes. As it can be seen, the voltage displays a steady-state behaviour with a period of around 84 ms for this given set of frequencies and amplitudes.
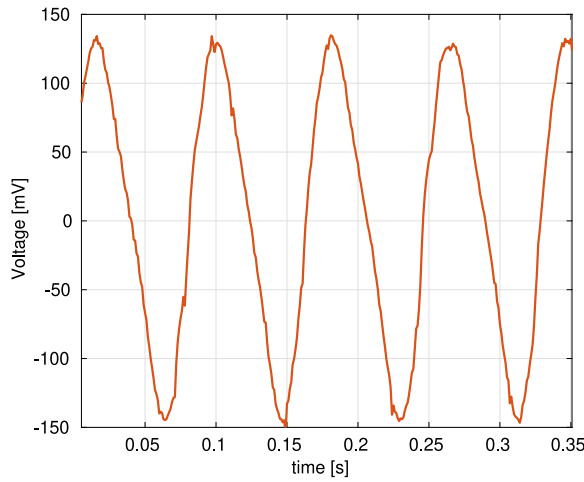
Fig. 5. Output voltage with frequencies of 3.5 Hz and 6 Hz on the semi minor and major axes respectively and amplitude of 4 mm on both axes.
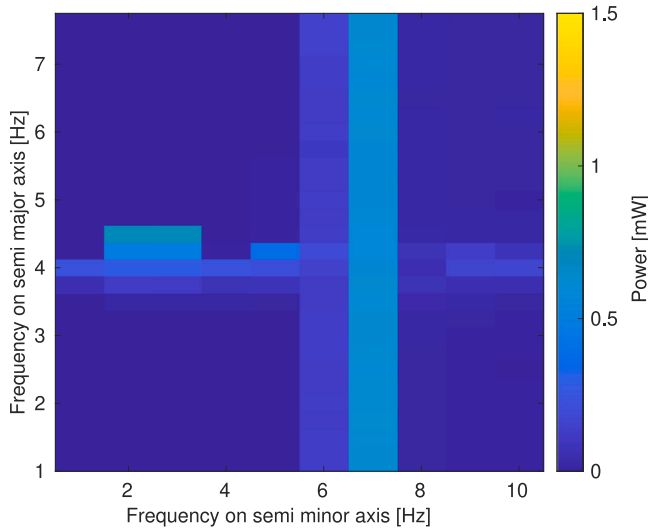

Fig. 6. Output power with a resistance load of 33 Ω and the coil windings connected in series. The amplitude displacement in both platforms of the XY shaker is 2 mm.

Fig. 7. Output power with a resistance load of 33 Ω and the coil windings connected in series. The amplitude displacement in both platforms of the XY shaker is 4 mm.
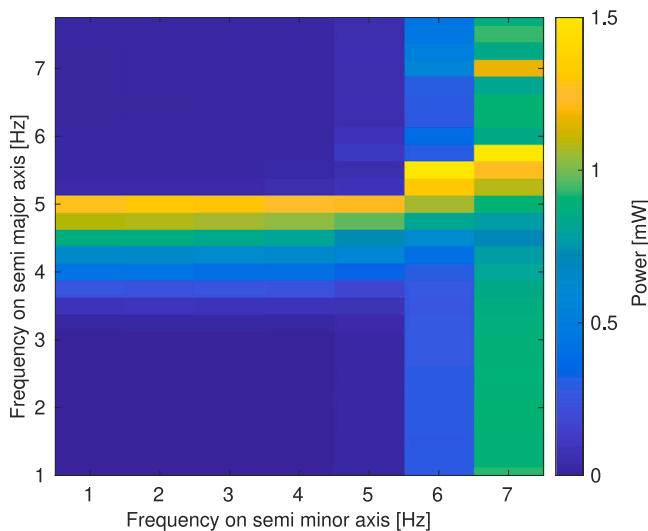
The output voltage signal of the harvester is periodic in nature, as expected for such harvesters. In order to use the harvester energy, for instance, to power sensors or IoT devices, the voltage signal must be rectified [35], and probably boost up [36].

From the Resistive-Inductive electrical equivalent circuit, or simply RL-circuit, the internal coil winding inductance is neglected due to the low impedance at the chosen low testing frequencies. Therefore, the load resistance R_L connected to the harvester only matches the total internal resistance of the two coil windings, which gives 33 Ω, and the output power P_o is calculated with Eq. (10),

$$P_o = \frac{V_{rms}^2}{R_L},\qquad(10)$$

where V_{rms} is the root-mean-cube voltage over the connected load R_L. For all frequencies and an shaking amplitude in both directions of 2 mm, the produced power is shown in Fig. 6, while for a shaking amplitude of 4 mm, the power is shown in Fig. 7. As noted previously, for each frequency, the harvester starts from rest. In each figure, there are two resonant frequencies, one related to the semi-major axis of the confining ellipse, which is in the range of 4 Hz to 5 Hz, and the other to the semi-minor axis, in the range of 6 Hz to 8 Hz. Note that at resonance, especially for the resonance on the semi minor axis, the power is not a function of the frequency of the semi-major axis because the power is completely dominated by the frequency response in the semi-minor axis. Said in another way, the movement of the free-to-move magnet is dominated by the resonance in the semi-minor direction. Furthermore, as the harvester behaves as a nonlinear resonator, the power is generated in a range of frequencies rather than an specific frequency. Moreover, by comparing Fig. 6 with Fig. 7, it can be seen that the resonant frequencies shift as the displacement amplitude of the external source increases, as expected for a nonlinear resonator. For this experiment where the axes of the confining ellipse are aligned with the axes of vibrations, the 2D-EMVEH harvester behaves somewhat like two independent 1D-EMVEHs vibrating along the $x-$ and $y-$direction respectively. However, this is a consequence of the aligned movement and the symmetric placement of the coil windings with respect to this movement. Subsequently, the behaviour of the 2D-EMVEH is explored when this alignment between harvester and vibrations is not present.

However, before studying this, it is crucial to understand the actual movement of the free magnet, i.e. the ring magnet, in the system when this is vibrating. Therefore, the movement of the ring magnet was recorded using a GOPRO Hero 8 camera through the transparent top plate of the 2D-EMVEH. The camera is attached to a rigidly connected holder to the harvester so that the relative movement between the ring magnet and the harvester can directly be observed. The video recording is then analysed to trace the trajectory described by the ring magnet. The resulting curve is shown in the bottom panel of Fig. 8 for a frequency of 7 Hz in the semi-major axis direction and a frequency of 4 Hz for the semi-minor axis, and 4 mm amplitude in both platforms. In addition, the bottom panel of Fig. 8 shows a still frame from the video with a portion of the trajectory overlapped. The entire tracking video is available in the data repository for this work [37], as also described subsequently. The trajectory can be compared to a Lissajous curve [38]:

$$\begin{aligned} x(t) &= x_0 + A_x\cos(2\pi f_x t + \phi_x) \\ y(t) &= y_0 + A_y\cos(2\pi f_y t + \phi_y) \end{aligned}\qquad(11)$$

This is the movement that would be expected for a harmonic two-dimensional oscillator without any nonlinear term. In reality, the 2D harvester is governed by a nonlinear equation of motion, so a perfect match between the Lissajous curve and the traced trajectory is not expected. The fitting parameters appearing in Eq. (11) are obtained by minimizing the root mean square Δ_{rms} of the difference between the experimental data points and the Lissajous model. This figure of merit can also be used to quantify the goodness of the fit. For $x(t)$ a value of $\Delta_{rms} = 0.63$ mm is obtained, and for $y(t)$ the value is $\Delta_{rms} = 1.79$ mm,
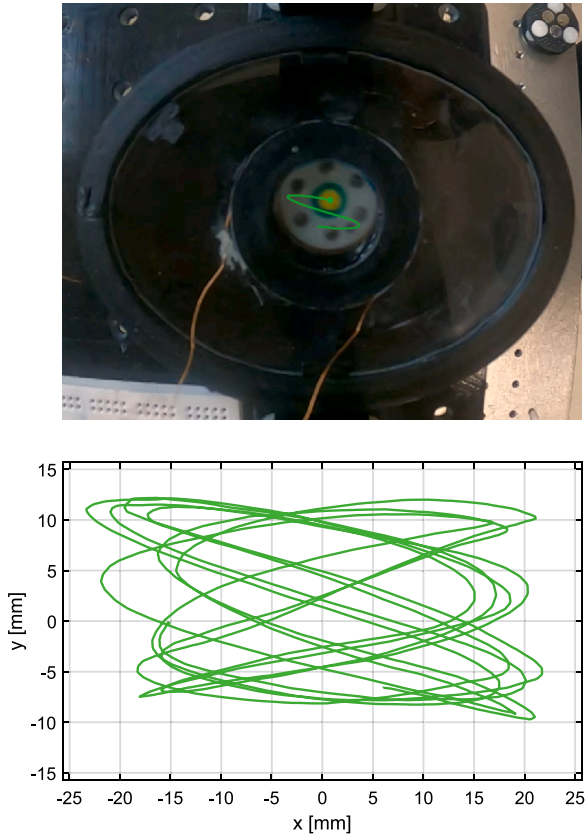
Fig. 8. Top panel: still frame from the recording of the motion of the ring magnet. A portion of the trajectory is displayed as a green curve. Bottom panel: tracing of the trajectory of the ring magnet. (For interpretation of the references to colour in this figure legend, the reader is referred to the web version of this article.)

which are both in reasonably good agreement. It is also interesting to compare the frequencies f_x and f_y obtained from the fitting with the corresponding frequencies used to control the XY-shaker. From the fitting $f_x/f_y = 1.751$ is obtained, while from the input frequencies, i.e. 7 Hz and 4 Hz, $f_x/f_y = 1.750$ is obtained, again showing a good agreement between the model and the experimental data.

3.2. 1D vibrations

Following the two-dimensional vibrational experiments discussed above, it was also of interest to examine the behaviour of the harvester when it was subjected only to one-dimensional vibrations, especially when these were not aligned with the axis of the harvester ellipse. Therefore, an experiment was performed where the excitation frequency of only the top platform in the XY-shaker was changed, while the bottom platform was kept static; i.e., a one-dimensional vibration experiment was performed. However, for each experiment the angle between the semi-major axis of the harvester and the motion direction of the top platform were varied. Experiments were done in steps of 15° and with amplitudes of 2 mm and 4 mm. Precisely, 0° alignment corresponds to the semi-major axis aligned with the motion direction, and 90° corresponds to the semi-major axis perpendicular to the motion direction as shown in Fig. 9.

For the case of 2 mm motion amplitude, Fig. 10 shows that the system reaches the resonance frequency associated with the semi-minor axis at 7 Hz, similar to what was depicted in Fig. 6. Furthermore, it shows how much power the harvester can generate when the external vibration source is not aligned with the semi-major axis of the elliptical holder. In this particular case, the elliptical harvester produces up
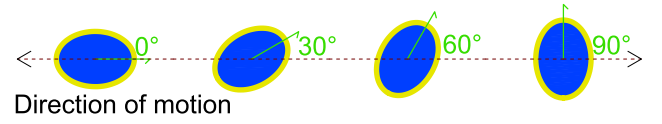

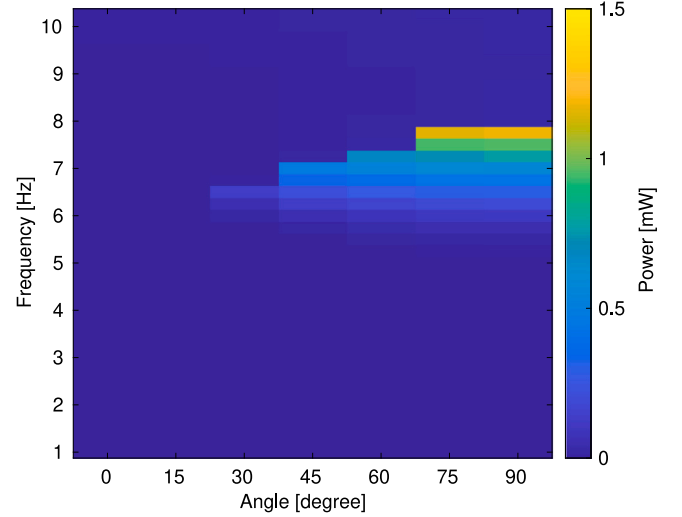Fig. 9. Angular position of the harvester with respect to the motion axis.

Fig. 10. Output power with respect to frequency and angular position of the harvester. Load resistance of 33 Ω and coil windings connected in series. The amplitude displacement in the top platform of the XY shaker is 2 mm.

to 0.1 mW when its semi-major axis has an angular position of 30° with respect to the direction of the vibration ambient source. On the other hand, when the motion amplitude is increased to 4 mm, the resonance frequency shifts from 5 Hz to 7.5 Hz when the angular position changes from 0° to 90° with respect to the semi-major axis, as shown in Fig. 11. This means the prototype can harvest energy at two resonance frequencies which depends on the orientation of the harvester to the motion direction, giving a maximum output power of approximately 1.5 mW at 7.75 Hz when the harvester has an angular position of 45°. Note that while the harvester is started from rest for every single frequency pair measured, the power landscape as function of frequencies is continuous. This means that starting at given frequency and then changing the frequency will result in a continuous transition to the state.

Here the behaviour of the 2D-EMVEH is markedly different from that of two independent 1D-EMVEHs, which could never be made to harvest energy if their axes of motion were not aligned to the source of vibrations. For example, for the case of the amplitude of 4 mm and an angular position of 45°, there are two resonant peaks in frequency at both 4.75 Hz and 7.75 Hz. Such double resonances are not traditionally seen in 1D-EMVEHs, although some systems do display such behaviour [39]. Thus, the 2D-EMVEH system has a unique benefit as an energy harvesting platform.

3.3. Modelling the 2D-EMVEH

The physics derived for the 2D-EMVEH in Section 2.1 allows the behaviour of the system to be modelled. To model the system and integrate equations (1) and (2), first, the magnetic restoring force and induced magnetic flux on the coil windings were obtained from the finite element method software Comsol. The equation solved in the FEM framework is the magnetic scalar potential equation

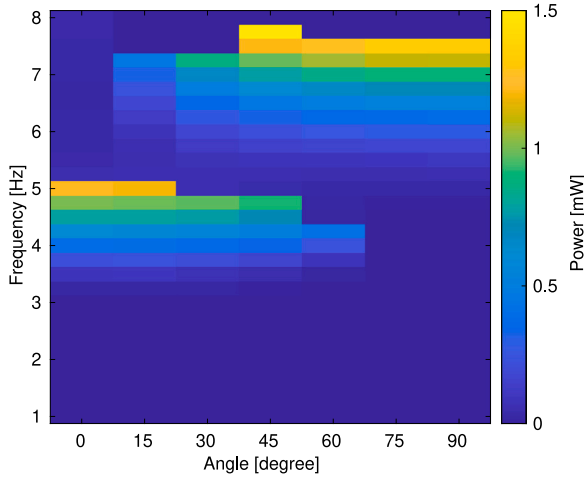$$-\nabla \cdot (\mu_0 \mu_r \nabla V_\mathrm{m}) = 0 \ . \tag{12}$$

Fig. 11. Output power with respect to frequency and angular position of the harvester. Load resistance of 33 Ω and coil windings connected in series. The amplitude displacement in the top platform of the XY shaker is 4 mm.
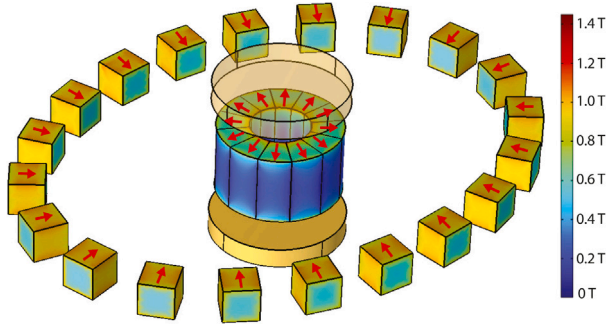

Fig. 12. Magnets distributed elliptically, with the ring magnet and coil windings in the centre. The red arrows indicate the direction of magnetization of the magnets. The coils are shown as two discs, with the top coil being slightly transparent.

Here μ_0 is the permeability of free space, μ_r is the relative permeability, which is assumed to be equal to 1, and V_m is the magnetic scalar potential. The magnetic field is then calculated as $-\nabla V_m = \mathbf{H}$.

To determine the force on the free-to-move magnet, Maxwell's stress tensor, $\mathbb{T}$, must be integrated across the surface covering this [40]

$$\mathbf{F} = \oint_{S'} \mathbb{T} \cdot d\mathbf{a} \tag{13}$$

where S' denotes the closed surface surrounding the free-to-move magnet and $d\mathbf{a}$ is an area element of this. With no electrical fields, Maxwell's stress tensor is given by

$$T_{ij} = \frac{1}{\mu_0} \left(B_i B_j - \frac{1}{2} \delta_{ij} B^2 \right), \tag{14}$$

where $\mathbf{B} = (B_x, B_y, B_z)$ is the magnetic flux density. This integration is automatically done in the Comsol framework.

An illustration of the simulation for computing the force and flux is shown in Fig. 12, which depicts the 3D simulation of the harvester in Comsol, where the position of the ring magnet was swept in steps of 1 mm from the centre to the edge of the elliptically-distributed set of cube magnets. The computed components of the magnetic restoring force on the x- and y-axes are shown in Figs. 13 and 14; likewise, the magnetic flux on the winding coil is illustrated in Fig. 15.

The obtained force and flux were employed to integrate equations (1) and (2) using a standard Runge Kutta ode45 solver in Matlab, calculating the produced power of the harvester. Fig. 16 shows the calculated total induced voltage of the series-connected winding coils
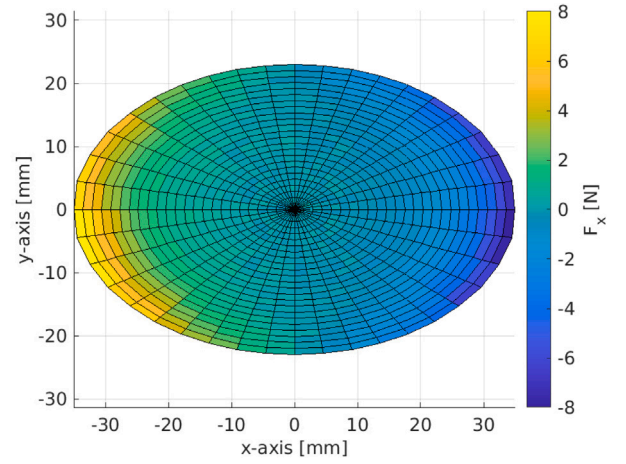

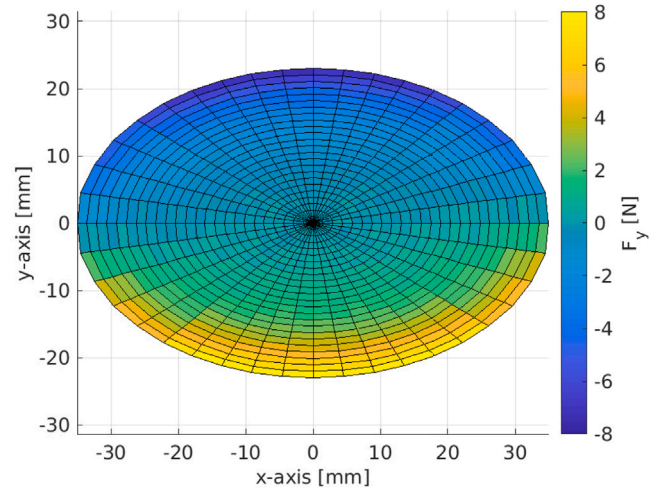**Fig. 13.** X-axis component of the magnetic restoring force.

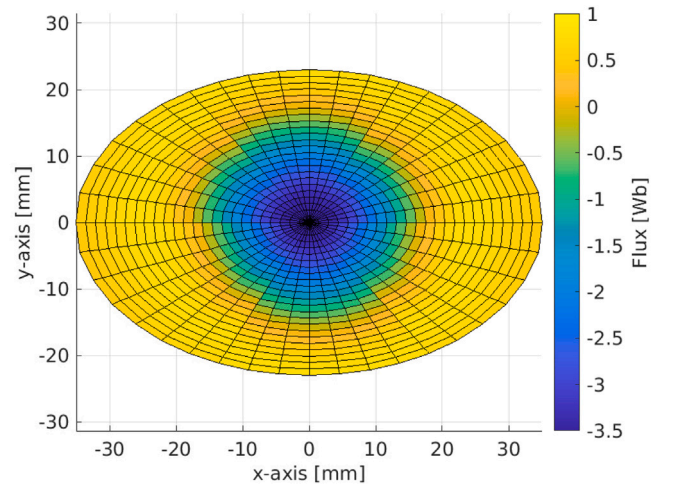**Fig. 14.** Y-axis component of the magnetic restoring force.

Fig. 15. Magnetic flux on the fixed 280-turn coil winding as a function of the position of the free-to-move magnet.

for the case of an external frequency of 3.25 Hz and 6 Hz aligned to the semi-major and semi-minor axes, respectively, and amplitude of 4 mm for both axes. As can be seen, the model results match very well
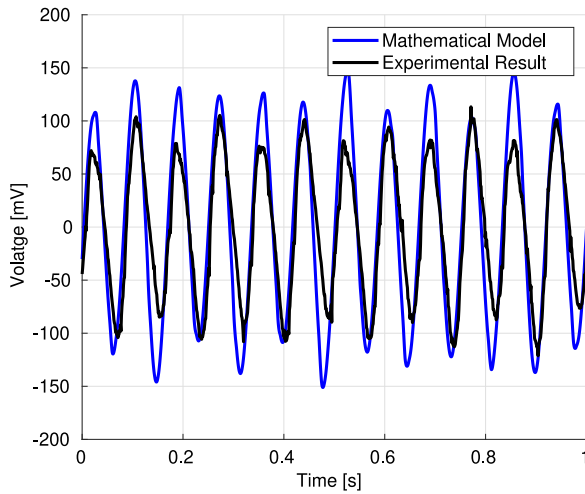
Fig. 16. Output voltage of the two coil windings connected in series. The motion frequency is 3.25 Hz on the semi-mayor axis and 6 Hz on the semi-minor axis, and the motion amplitude on both axes is 4 mm.

Fig. 17. Four NMOS Rectifier (4NR) circuit.

Fig. 18. Open circuit and rectified voltage.

with the measured experimental voltages. The only free parameter in the model is the mechanical friction coefficient, which was fitted to 0.08 kg/s. As this work studies the overall design and dynamics of the 2D elliptically-shaped harvester, further simulations are not pursued in this work. However, as the dynamics of the system can be modelled using a 2D EMVEH model as demonstrated here, a future 2D harvester design can be optimized using this approach.

4. Discussion

It is desirable to compare the power produced by the 2D-EMVEH system to the traditional 1D-EMVEH systems. In the review study performed in Ref. [6], the power density of the 1D harvesters is listed according to their different topologies. The results show a power density up to 4500 μW/cm^3 for the harvester described in Ref. [41], and a power density of 0.34 μW/cm^3 for the one in Ref. [42]. However, the vibration testing conditions are different for every simple prototype; for instance, the acceleration peak values were 4.3 g and 0.07 g, respectively, in the two previous referenced devices. Nonetheless, this information gives an idea of how much power a 1D harvester can generate. In the case of the 2D-EMVEH tested here, for a motion amplitude of 4 mm, the acceleration in the semi-major and semi-minor axes are 0.79 g and 0.53 g maximally, respectively. This gives a total power density of approximately 56 μW/cm^3. However, this outcome cannot be directly compared with Ref. [41] because that prototype reaches resonance at around 40 Hz. On the other hand, the harvester in Ref. [42] was studied at frequencies at the range of human motion; i.e. up to 10 Hz, which is precisely the condition where the 2D-EMVEH was tested. Thus the performance of the 2D-EMVEH shows a clear potential for high power vibrational harvesting, especially considering that the harvester presented in this work has not been optimized with respect to the size and placement of the coil windings in the harvester. Compared to the harvester presented in Ref. [29], which produced a maximum power of 27 mW at an amplitude of 2 mm, the power produced here of ~1 mW is substantially less. However, the harvester in Ref. [29], while of the same size as the device presented here, contains many more magnets and is a more complicated design. The magnetization direction of the moving magnet was also optimized with respect to the coils in that work, which has not been done here.

It is always desirable to harvest as much power as possible from ambient vibrations. For the present system, the harvested power could be increased by reducing the gap between the pole faces of the ring magnet and the top and bottom coil windings. This would be possible if
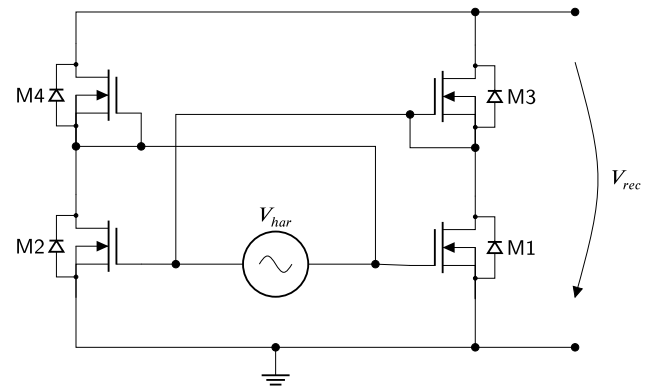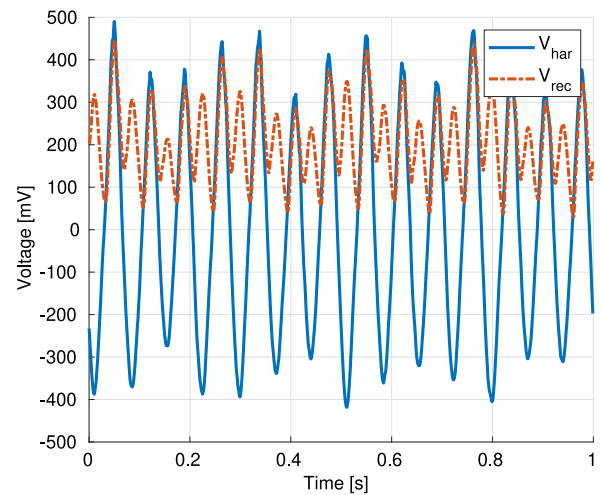
smaller bearings could be found, or the confining plates could be made of very low friction material. However, it should also be mentioned that increasing the flux through the coil windings, either by moving them closer to the ring magnet or by making the coil windings larger, e.g. increasing the number of windings, will affect the movement of the ring magnet, as the coil windings damp its motion. Therefore, determining the optimal coil winding size for a given harvester is not trivial. However, here the goal is to demonstrate that an impressive amount of power can be harvested from the 2D-EMVEH, and the optimization of the coil winding sizes will be discussed in a subsequent job.

Finally, there is no use of the generated power from the harvester if this cannot be converted to direct current. For this, a rectification stage is required and implemented as in Ref. [43]. The four N-channel MOSFET bridge (4NMOS) shown in Fig. 17 has a low drop voltage, creating a suitable conditioning circuit for energy harvesters. The results of Fig. 18 depicted the AC harvester generated voltage and the rectified voltage by the 4NMOS when the elliptically-shaped harvester is tested with an amplitude motion of 4 mm in both axes, and motion frequencies of 5 Hz and 7 Hz on the x- and y-axis respectively. Note that the power can nicely be rectified. An energy storage stage such as a capacitor will also be necessary for a final application, but this is typically chosen based on the application.

5. Conclusion

A two-dimensional elliptically shaped electromagnetic vibration energy harvester was presented and experimentally characterized to supply energy to low-power devices. The prototype was tested in an

XY-shaker with a sweep frequency from 1 Hz to 10 Hz in two directions simultaneously. The results showed that the 2D-EMVEH has two resonance frequencies at 4.5 Hz and 7 Hz, associated with its semi-major and semi-minor axes due to its elliptical shape. The device was also shown to have nonlinear hardening resonator behaviour, demonstrated by increased resonance frequency with increasing source amplitude. Finally, the behaviour of the harvester was also characterized when it was subjected to 1D vibration. Here the device could produce maximally 1.5 mW power, with the actual power depending on the harvester angular position with respect to the motion direction of the ambient vibration source. However, power was harvested at all angular vibrations, unlike traditional 1D electromagnetic harvesters.

CRediT authorship contribution statement

Carlos Imbaquingo: Methodology, Experimental work, Simulation, Writing, Visualization. **Christian Bahl:** Conceptualization, Writing. **Andrea R. Insinga:** Motion data tracking, Writing. **Rasmus Bjørk:** Conceptualization, Simulation, Writing.

Declaration of competing interest

The authors declare the following financial interests/personal relationships which may be considered as potential competing interests: Rasmus Bjoerk reports financial support was provided by Independent Research Fund Denmark. Carlos Imbaquingo reports a relationship with Technical University of Denmark that includes: employment. Christian Bahl reports a relationship with Technical University of Denmark that includes: employment. Andrea Roberto Insinga reports a relationship with Technical University of Denmark that includes: employment. Rasmus Bjoerk reports a relationship with Technical University of Denmark that includes: employment.

Data availability

All data presented in this manuscript in the form of the measured voltage curves as function of time for the different experiments are directly available from [37].

Acknowledgements

References

[1] Elda M. Melchor-Martínez, Rodrigo Macias-Garbett, Alonso Malacara-Becerra, Hafiz M.N. Iqbal, Juan Eduardo Sosa-Hernández, Roberto Parra-Saldívar, Environmental impact of emerging contaminants from battery waste: A mini review, Case Stud. Chem. Environ. Eng. 3 (November 2020) (2021) 100104.

[2] Iftikhar Ahmad, Lim Meng, Ahmed M. Abdelrhman, Syed Asad, M.S. Leong, Scopes , challenges and approaches of energy harvesting for wireless sensor nodes in machine condition monitoring systems : A review, Measurement 183 (April) (2021) 109856.

[3] Shashank Priya, Daniel J. Inman, Energy Harvesting Technologies, Springer US, 2009, pp. 1–517.

[4] Clemens Cepnik, Roland Lausecker, Ulrike Wallrabe, Review on electrodynamic energy harvesters - a classification approach, Micromachines 4 (2013) 168–196.

[5] Elena, El Aroudi Blokhina, Nonlinearity in Energy Harvesting Systems, Springer International Publishing, 2016.

[6] Pedro Carneiro, Marco P. Soares dos Santos, André Rodrigues, Jorge A.F. Ferreira, José A.O. Simões, A. Torres Marques, Andrei L. Kholkin, Electromagnetic energy harvesting using magnetic levitation architectures: A review, Appl. Energy 260 (2020) 114191.

[7] Hieu Tri Nguyen, Dentcho A. Genov, Hamzeh Bardaweel, Vibration energy harvesting using magnetic spring based nonlinear oscillators: Design strategies and insights, Appl. Energy 269 (2020) 115102.

[8] B.P. Mann, N.D. Sims, Energy harvesting from the nonlinear oscillations of magnetic levitation, J. Sound Vib. 319 (1–2) (2009) 515–530.

[9] Raul Morais, Nuno M. Silva, Paulo M. Santos, Clara M. Frias, Jorge A.F. Ferreira, Antonio M. Ramos, Jose A.O. Simoes, Jose M.R. Baptista, Manuel C. Reis, Double permanent magnet vibration power generator for smart hip prosthesis, Sensors Actuators A 172 (1) (2011) 259–268, Eurosensors XXIV, Linz, Austria, 5-8 September 2010.

[10] Marco P Soares Dos Santos, Jorge AF Ferreira, José AO Simões, Ricardo Pascoal, João Torrão, Xiaozheng Xue, Edward P Furlani, Magnetic levitation-based electromagnetic energy harvesting: a semi-analytical non-linear model for energy transduction, Sci. Rep. 6 (1) (2016) 1–9.

[11] Kangqi Fan, Meiling Cai, Haiyan Liu, Yiwei Zhang, Capturing energy from ultra-low frequency vibrations and human motion through a monostable electromagnetic energy harvester, Energy 169 (2019) 356–368.

[12] Carlos Enrique Imbaquingo, Marco Beleggia, Andrea Roberto Insinga, Christian RH Bahl, Brian Mann, Rasmus Bjørk, Analytical force and flux for a 1-D electromagnetic vibration energy harvester, IEEE Trans. Magn. 56 (11) (2020) 1–6.

[13] Haojun Liao, Tingcong Ye, Yu Pang, Ciaran Feeney, Lei Liu, Zhengmin Zhang, Chitta Saha, Ningning Wang, Modelling and optimization of a magnetic spring based electromagnetic vibration energy harvester, J. Electr. Eng. Technol. (2021) 1–12.

[14] Tra Nguyen Phan, Jesus Javier Aranda, Bengt Oelmann, Sebastian Bader, Design optimization and comparison of cylindrical electromagnetic vibration energy harvesters, Sensors 21 (23) (2021) 7985.

[15] Mingyuan Gao, Yuan Wang, Yifeng Wang, Ye Yao, Ping Wang, Yuhua Sun, Jieling Xiao, Modeling and experimental verification of a fractional damping quad-stable energy harvesting system for use in wireless sensor networks, Energy 190 (2020) 116301.

[16] Tobias Willemoes Jensen, Andrea R Insinga, Johan Christian Ehlers, Rasmus Bjørk, The full phase space dynamics of a magnetically levitated electromagnetic vibration harvester, Sci. Rep. 11 (1) (2021) 1–15.

[17] Shuo Cheng, Naigang Wang, David P. Arnold, Modeling of magnetic vibrational energy harvesters using equivalent circuit representations, J. Micromech. Microeng. 17 (11) (2007) 2328.

[18] L.B. Zhang, H.L. Dai, Y.W. Yang, L. Wang, Design of high-efficiency electromagnetic energy harvester based on a rolling magnet, Energy Convers. Manage. 185 (2019) 202–210.

[19] Yifeng Wang, Shoutai Li, Mingyuan Gao, Huajiang Ouyang, Qing He, Ping Wang, Analysis, design and testing of a rolling magnet harvester with diametrical magnetization for train vibration, Appl. Energy 300 (2021) 117373.

[20] Takahiro Sato, Hajime Igarashi, A chaotic vibration energy harvester using magnetic material, Smart Mater. Struct. 24 (2) (2015) 025033.

[21] Yunhee Choi, Suna Ju, Song Hee Chae, Sangbeom Jun, Chang-Hyeon Ji, Low-frequency vibration energy harvester using a spherical permanent magnet with controlled mass distribution, Smart Mater. Struct. 24 (6) (2015) 065029.

[22] Bin Bao, Shaoyi Zhou, Quan Wang, Interplay between internal resonance and nonlinear magnetic interaction for multi-directional energy harvesting, Energy Convers. Manage. 244 (2021) 114465.

[23] Xiaobiao Shan, Guangdong Sui, Haigang Tian, Zhaowei Min, Ju Feng, Tao Xie, Numerical analysis and experiments of an underwater magnetic nonlinear energy harvester based on vortex-induced vibration, Energy (2021) 122933.

[24] M. Salauddin, M.S. Rasel, J.W. Kim, Jae Y. Park, Design and experiment of hybridized electromagnetic-triboelectric energy harvester using halbach magnet array from handshaking vibration, Energy Convers. Manage. 153 (2017) 1–11.

[25] Manuel Gutierrez, Amir Shahidi, David Berdy, Dimitrios Peroulis, Design and characterization of a low frequency 2-dimensional magnetic levitation kinetic energy harvester, Sensors Actuators A 236 (2015) 1–10.

[26] S. Palagummi, F.G. Yuan, A bi-stable horizontal diamagnetic levitation based low frequency vibration energy harvester, Sensors Actuators A 279 (2018) 743–752.

[27] Benjamin J. Bowers, David P. Arnold, Spherical, rolling magnet generators for passive energy harvesting from human motion, J. Micromech. Microeng. 19 (9) (2009).

[28] Ken Sasaki, Yuji Osaki, Jun Okazaki, Hiroshi Hosaka, Kiyoshi Itao, Vibration-based automatic power-generation system, Microsyst. Technol. 11 (8–10) (2005).

[29] Carlos Imbaquingo, Christian Bahl, Andrea R Insinga, Rasmus Bjørk, A two-dimensional electromagnetic vibration energy harvester with variable stiffness, Appl. Energy 325 (2022) 119650.

[30] Robert Weinstock, On a fallacious proof of Earnshaw's theorem, Amer. J. Phys. 44 (4) (1976) 392–393.

[31] Krzysztof Kecik, Marcin Kowalczuk, Effect of nonlinear electromechanical coupling in magnetic levitation energy harvester, Energies 14 (9) (2021) 2715.

[32] Arthur Eugene. Fitzgerald, Charles. Kingsley, Stephen D. Umans, Electric Machinery, McGraw-Hill, 2003, p. 688.

[33] R. Olaru, R. Gherca, Generator with levitated magnet for vibration energy harvesting, Int. J. Appl. Electromagn. Mech. 42 (3) (2013) 421–435.

[34] Igor Neri, Flavio Travasso, Riccardo Mincigrucci, Helios Vocca, Francesco Orfei, Luca Gammaitoni, A real vibration database for kinetic energy harvesting application, J. Intell. Mater. Syst. Struct. 23 (18) (2012) 2095–2101.

[35] A Santiago Rodriguez, N Garraud, D Alabi, A Garraud, DP Arnold, A simple passive 390 mV ac/dc rectifier for energy harvesting applications, in: Journal of Physics: Conference Series, Vol. 1407, IOP Publishing, 2019, 012018.

[36] Shuo Cheng, Ying Jin, Yuan Rao, David P. Arnold, An active voltage doubling AC/DC converter for low-voltage energy harvesting applications, IEEE Trans. Power Electron. 26 (8) (2010) 2258–2265.

[37] C. Imbaquingo, C. Bahl, A.R. Insinga, R. Bjørk, Data for article two-dimensional elliptically shaped electromagnetic vibration energy harvester, 2022, http://dx. doi.org/10.11583/DTU.21548196, data.dtu.dk.

[38] H.C. Richards, On the harmonic curves known as lissajous figures, J. Franklin Inst. B 153 (1903) 269–283.

[39] Philip Holm, Carlos Imbaquingo, Brian P. Mann, Rasmus Bjørk, High power electromagnetic vibration harvesting using a magnetic dumbbell structure, J. Sound Vib. 546 (2023) 117446.

[40] D.J. Griffiths, Introduction to Electrodynamics, Pearson Education, 2014, p. 604.

[41] P. Constantinou, P.H. Mellor, P. Wilcox, A model of a magnetically sprung vibration generator for power harvesting applications, in: 2007 IEEE International Electric Machines Drives Conference, Vol. 1, 2007, pp. 725–730.

[42] D.F. Berdy, D.J. Valentino, D. Peroulis, Kinetic energy harvesting from human walking and running using a magnetic levitation energy harvester, Sensors Actuators A 222 (2015) 262–271.

[43] A. Santiago Rodriguez, N. Garraud, D. Alabi, A. Garraud, D.P. Arnold, A simple passive 390 mV ac/dc rectifier for energy harvesting applications, J. Phys. Conf. Ser. 1407 (1) (2019).

Carlos Imbaquingo completed his Engineer's degree in Electronics and Control Systems at the National Polytechnic School, Quito, Ecuador, in 2010, followed by a M.Sc. in Renewable Energies and Energy Efficiency at Universidad de Zaragoza, Saragossa, Spain in 2013; and another M.Sc. in Wind Power Systems at Aalborg University, Aalborg, Denmark, in 2018. He received his Ph.D. degree from the Department of Energy Conversion and Storage, Technical University of Denmark, Copenhagen, Denmark, in 2022.

He is currently working as a postdoctoral researcher at DTU Energy, and his research is focused on conditioning circuits for energy storage systems of energy harvesters.

Christian Bahl is an associate professor at the Technical University of Denmark. He received his M.Sc. degree in solid-state physics from the University of Copenhagen in 2003. Following this, he received a Ph.D. degree in experimental nano-magnetism from the Technical University of Denmark in 2006. Since then, he has worked on studies of magnetic materials, energy applications including magnetic materials, and heat and mass transfer in thermal systems.

Andrea Roberto Insinga is an Assistant Professor at the Department of Energy Conversion and Storage at the Technical University of Denmark (DTU). His main research interests are numerical modelling of magnetic and piezoelectric materials, design optimization, and quantum thermodynamics. He received his Ph.D. from the Technical University of Denmark in 2016.

Rasmus Bjørk is a Professor and Head of the Section for Continuum Modelling and Testing at the Department of Energy Conversion and Storage at the Technical University of Denmark (DTU). His research is focused on permanent magnets, magnetostatics and micromagnetism, including both experiments and modelling, with a special focus on energy applications of these research areas. He received his Ph.D. from the Technical University of Denmark in 2010.